Journal of the Korean Nuclear Society
Volume 24, Number 3, September 1992

Measurements of Turbulent Flow in 5×5 PWR Rod Bundles With Spacer Grids

Sun Kyu Yang, Heung June Chung, Se Young Chun, and Moon Ki Chung
Korea Atomic Energy Research Institute

(Received February 8, 1992)

지지격자를 갖는 5×5 PWR 봉다발에서의 난류유동 측정

양선규 · 정흥준 · 천세영 · 정문기

(1992. 2. 8 접수)

Abstract

The study on the velocity distribution and the pressure drop characteristic of the nuclear fuel assembly is of importance for the thermal hydraulic design and safety analysis. The purpose of this experimental study is to investigate the hydraulic mixing behind the different kinds of spacer grids in the flow of rod bundles. In this study, the detailed hydraulic characteristics in subchannels of 5×5 PWR(Pressurized Water Reactor) rod bundles were measured using one-component He-Ne LDV(Laser Doppler Velocimeter).

Measurements of the axial velocity, turbulent intensities and pressure drops were performed. Lateral velocity, turbulent intensities and Reynolds shear stress were also measured by adjusting LDV alignment. Friction factors in rod bundles and loss coefficients for spacer grids were evaluated from the measured pressure drops.

Hydraulic mixing performance for different kinds of spacer grids could be investigated by estimating the turbulent cross-flow mixing rates between neighboring subchannels.

요 약

핵연료 집합체의 속도분포, 압력강하는 열수력 설계와 안전해석에 중요하다. 본 실험적 연구의 목적은 봉다발 지지격자 하류에서의 수력학적 혼합을 고찰하는데 있다. 이 연구에서 가압경수로형 5×5 봉다발 부수로의 상세한 수력학적 특성들을 1차원 He-Ne LDV를 이용하여 측정하였다.

축방향 유속, 난류강도와 압력강하를 주로 측정하였고 LDV의 정렬을 조정하여 측방향의 유속, 난류강도, Reynolds 전단응력 등도 역시 측정하였다. 봉다발의 마찰계수와 지지격자의 손실계수는 측정된 압력강하로부터 평가하였다.

서로 다른 종류의 지지격자의 수력학적 혼합성능을 이웃하는 부수로간에서의 난류 횡류 혼합률을 예측함으로써 고찰할 수 있었다.

1. Introduction

The study on the velocity distribution and the pressure drop characteristic of the nuclear fuel assembly is of importance for the thermal hydraulic design and safety analysis. The purpose of this experimental study is to investigate the hydraulic mixing behind the different kinds of spacer grids in the flow of rod bundles. In this study, the detailed hydraulic characteristics in subchannels of 5×5 PWR(Pressurized Water Reactor) rod bundles were measured using one-component He-Ne LDV(Laser Doppler Velocimeter) [1, 2].

Previous experimental studies on the flow characteristics of bare rod bundles can be reviewed from the Rehme's [3~6] and Hooper and Rehme's [7] studies. Of previous studies, Rowe et al. [8], Carajilescov and Todreas [9], Renksizbulut and Hadaller [10], and Vonka [11] performed experimental studies on bare rod bundle flows using LDV. Rowe et al., one of the earliest applications of LDV to subchannel flows, measured turbulent microscopic structures which were helpful to obtain a better understanding of cross-flow mixing between neighboring subchannels. Their results showed that rod gap spacing was the most significant geometric parameter affecting the flow structure. Decreasing the rod gap spacing increases the turbulence intensity, longitudinal macroscale, and the dominant frequency of turbulence. From evaluating the dominant frequency of turbulence, they suggested the presence of periodic flow pulsations in the gap region.

In this study, measurements of the axial velocity, turbulent intensities and pressure drops were performed. Lateral velocity, turbulent intensities and Reynolds shear stress were also measured by adjusting LDV alignment.

Friction factors in rod bundles and loss coefficients for spacer grids were evaluated from the measured pressure drops. The hydraulic mixing performance for different kinds of spacer grids was investigated by estimating the turbulent cross-flow mixing rates between neighboring subchannels. And, by obtaining the turbulent cross-flow mixing, mixing factors in subchannel analysis code can be predicted quantitatively.

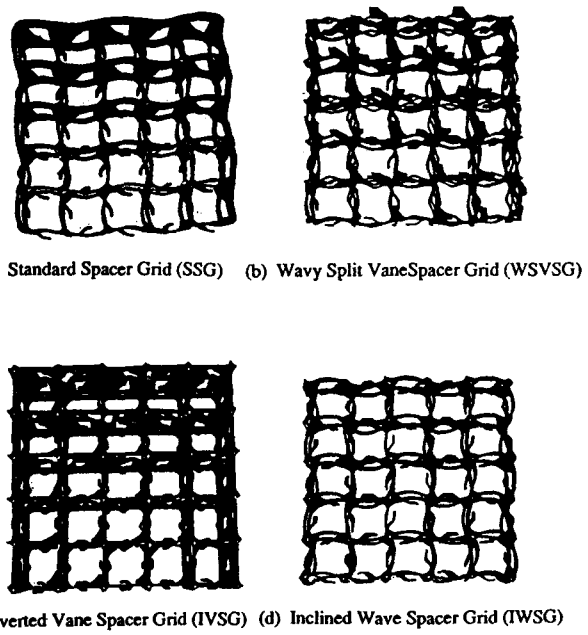

(a) Standard Spacer Grid (SSG) (b) Wavy Split VaneSpacer Grid (WSVSG)

(c) Inverted Vane Spacer Grid (IVSG) (d) Inclined Wave Spacer Grid (IWSG)

Fig. 1. The Photographies of Spacer Grids

The spacer grids tested in the present study are listed as follows :

-Standard Spacer Grid(SSG)
-Wavy Split Vane Spacer Grid(WSVSG)
-Inverted Vane Spacer Grid(IVSG)
-Inclined Wave Spacer Grid(IWSG)

The photographies of these spacer grids are shown in Figure 1(a), (b), (c), and (d).

2. Turbulent Phenomena in Rod Bundles

Subchannels of rod bundles consist of internal subchannel, wall subchannel and corner subchannel. Various types of subchannels having different flow passages and velocity fields have different flow characteristics.

Major features of turbulent phenomena in sub-

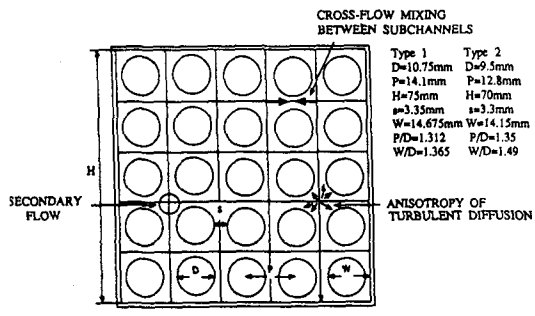

Fig. 2. 5×5 Rod Bundle Cross-Section Showing Turbulent Phenomena in Subchannel

channels include cross-flow mixing between subchannels [8], and secondary flow [11, 12] as shown in Figure 2.

Lateral turbulent energy and momentum exchange at the gap are based on a fluctuating mass exchange between neighboring subchannels. This is expressed as a fluctuating cross-flow mixing rate per unit length, w′ [13]. If the enthalpies and velocities of the neighboring subchannels are different, the exchange of energy and momentum flux will occur. The non-dimensionalized form of w′ can be expressed as [8]

$$\frac{w'}{G\,D_h}=\left(\frac{\nu_t}{U_{av}\,D_h}\right)\left(\frac{s}{\Delta y}\right) \tag{1}$$

where ν_t, G, D_h and U_{av} are turbulent eddy viscosity, mass flowrate, hydraulic diameter, and channel bulk velocity, respectively. This equation shows that the mixing parameter (w'/GD_h) can be expressed by the inverse turbulent Peclet number($\nu_t/U_{av}D_h$) and a geometric ratio parameter($s/\Delta y$). Mixing parameter (w'/GD_h) has been called the mixing Stanton number, St [8] based on hydraulic diameter, i.e.,

$$St=\frac{w'}{G\,D_h} \tag{2}$$

On the right hand side of Eq.(1), the undetermined value is turbulent eddy viscosity and the others are known as geometrical parameters and a flow condition. Turbulent eddy viscosity can be obtained by the two-equation model as proposed by Launder and Spalding [14], which is given by

$$\nu_t=C_\mu k^2/\epsilon \tag{3}$$

where C_μ is turbulent constant which is assumed to be 0.09, and k and ϵ are turbulent kinetic energy and dissipation rate respectively. k and ϵ can be evaluated by isotropic turbulence assumption. The small scale structure of turbulence tends to be isotropic. In this flow field, the relation, $\overline{u^2}=\overline{v^2}=\overline{w^2}$ is assumed. Thus, turbulent kinetic energy, k is

$$k=\frac{\overline{u_i^2}}{2}=\frac{\overline{3u^2}}{2} \tag{4}$$

The dissipation rate of turbulent kinetic energy, ϵ, is equal to [15]

$$\epsilon=15\nu\overline{\left(\frac{\partial u}{\partial x}\right)^2} \tag{5}$$

Using Taylor's hypothesis [16], the spatial gradient can be calculated from the time gradient which is easy to measure in the laboratory.

3. Experimental Facility and Method

3.1. Test-Loop

The test-loop is shown schematically in in Figure 3. It consists of two pumps, a storage tank.

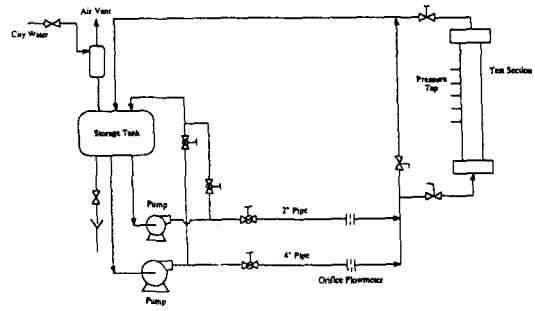

Fig. 3. Flow Diagram of Test Loop

Table 1. The Dimensions of Test Bundles and Flow Conditions

Characteristics	Type 1	Type 2
Diameter, D	10.75 mm	9.5 mm
Pitch, P	14.1 mm	12.8 mm
Housing Width, H	75 mm	70 mm
Rod Gap, s	3.35 mm	3.3 mm
Wall Distance, W	14.675mm	14.15mm
P/D	1.312	1.35
W/D	1.365	1.49
Hydraulic Diameter, D_h	11.74 mm	12.2 mm
Reynolds Number, Re	60800, 78300	74000

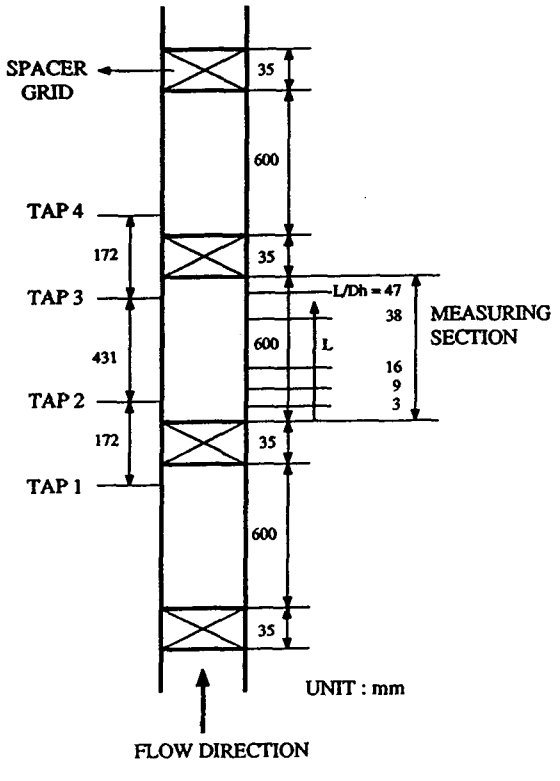

Fig. 4. Location of Spacer Grid, Pressure Taps, and Measuring Section

flow control valves, pipes, orifice flowmeters and a vertical flow channel. During experiments, water temperature in the loop was maintained at 30℃ by adjusting the feed and drain of water in the storage tank. The dimensions of test bundles and flow conditions for Type 1 and Type 2 are shown in Table 1. The 2m-long, 75mm(Type 1) and 70mm(Type 2)-square test section shown in figure 2 and 4 consists of 25 bare rods of 10.75mm(Type 1) and 9.5mm(Type 2) in diameter. The rods were arranged in a square array with P/D=1.312(Type 1), 1.35(Type 2) and W/D =1.365(Type 1), 1.49(Type 2).

The square housing is made of acryl to provide access for laser beams to the location where the velocity is to be measured.

3.2. Laser Doppler Velocimeter

The LDV measurements method is a non-intrusive optical techniques with good spatial resolution for accurate and fast determination of flow velocities in gases, liquids, and 2-phase flows. The LDV operates by measuring the velocity of very small particles suspended in the fluid and moving at the same speed. By crossing two beams from the same laser, a fringe (interference) pattern made up of dark and bright planes is generated within the measuring volume. A particle crossing this volume will generate a sequence of scattered light pulses(Doppler-Burst). The Doppler shift frequency is proportional to the component of the particle velocity perpendicular to the fringes. The relation between Doppler shift frequency, f_D and velocity component perpendicular to optical axis, $\tilde{u}$, is given by

$$f_D = 2\tilde{u} \sin \kappa / \lambda \quad (6)$$

where λ is the laser wavelength and κ is the half angle of laser beam intersection [17, 18].

The one-component He-Ne LDV system used in the present work was aligned by the dualbeam

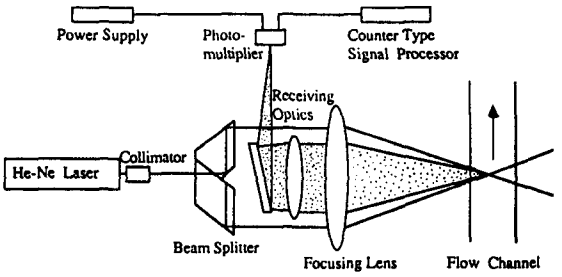

Fig. 5. Dual Beam LDV System With Backward Scattered Mode

backward scattered mode as shown schematically in Figure 5. The dual beam spacing is 50mm and the focal-length of focusing lens is 250mm. Silicon carbide particles, 1.5μm in diameter, 3.2g/cm^3 in density, 2.65 in refractive index, and 1.4 in geometric standard deviation, were added to obtain a better scattering signal.

3.3. Signal Processing

The signals from the photo-multiplier were processed using a counter type processor which consists of filters, a gain, a timer, a digital output, and a D/A(Digital to Analog) converter. The signal from digital output of signal processor was used to obtain the turbulent velocity and intensity using a personal computer. The dissipation rate of turbulent kinetic energy was evaluated by storing the analog signal from the signal processor into the transient recorder in connection with the personal computer, and processing the signal in the computer monitor.

4. Experimental Results and Discussion

4.1. Pressure Drops Measurements

The static pressure drops $\Delta P=P_4-P_1$ for an incompressible isothermal flow were measured over a length ΔL at the set flow rate Q with n spacer grids arranged over the measured length. Under this condition the measured pressure loss, ΔP, is made up of the friction loss in the rod bundle, ΔP_B, and the pressure drop at the spacer grid, ΔP_A, i.e.

$$\Delta P=\Delta P_B+n\Delta P_A \tag{7}$$

where n=2 in this study.

The pressure drop at this spacer grid is related to the bulk average fluid velocity, U_{av}, in the rod bundle[19].

$$\Delta P_A=C_B\rho/2U_{av}^2 \tag{8}$$

where C_B is the loss coefficient of the spacer grid and ρ is the fluid density. The Reynolds number Re of the flow in the rod bundle is expressed as

$$Re=U_{av}D_h/\nu \tag{9}$$

where ν is the kinematic viscosity, and the hydraulic diameter $D_h=4A/P_w$ with A as the flow cross-section and P_w as the wetted perimeter.

From the pressure drops, $\Delta P_{1-2}=P_2-P_1$ and $\Delta P_{3-4}=P_4-P_3$, loss coefficient, C_B, for the spacer grids can be calculated. Averaging lower spacer grid's pressure drop, ΔP_{1-2}, and upper spacer grid's pressure drop, ΔP_{3-4}, and using Eq.(8), loss coefficent can be estimated. Figure 6 shows loss coefficients for the spacer grids. The Inverted Vane Spacer Grid has the largest values.

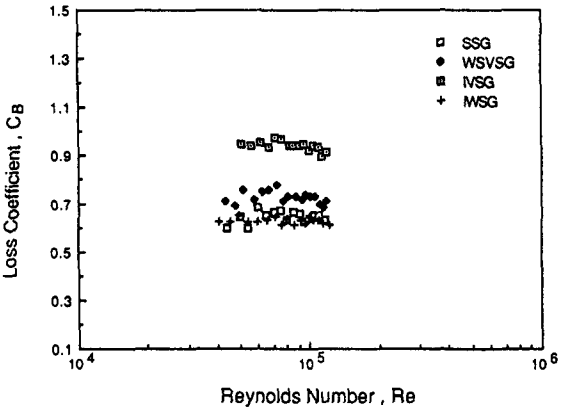

Fig. 6. Loss Coefficient for Spacer Grid (Type 3)

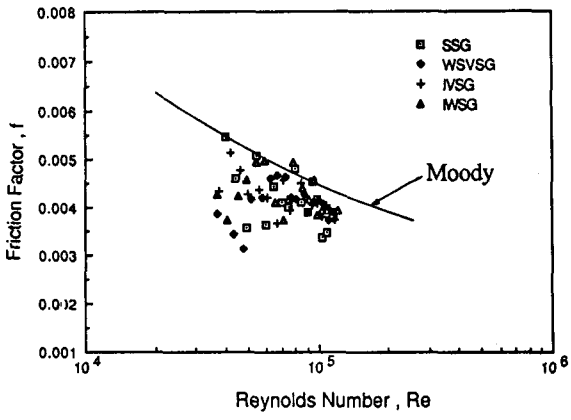

Fig. 7. Comparison of Fanning Friction Factors for Rod Bundles Flow With Those for Fully Developed Turbulent Flow in Smooth Wall Circular Tubes (Type 2)

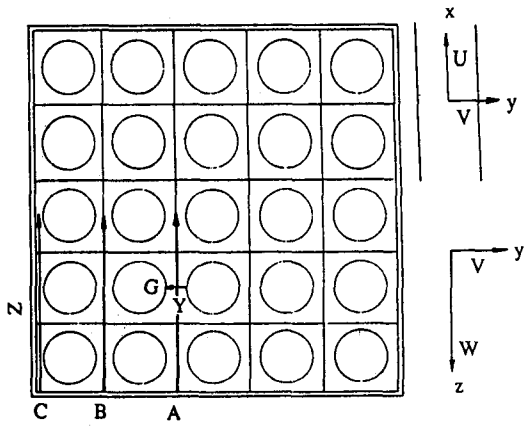

Fig. 8. Coordinate System and Measuring Path

Friction factors, f, rod bundles region were evaluated from measured pressure drops, ΔP_{2-3}, i.e.

$$f=-\Delta P_{2-3}/\Delta L D_h/(2\rho U_{av}^2) \quad (10)$$

In Figure 7, the friction factors were compared with the Moody's correlation for smooth tubes [20]. The results show that the friction factors for rod bundles are less than the values given by Moody's curve. The reason is not clear since the friction factors for rod bundles depend on the various kinds of geometric parameters such as P/D, W/D, and the type of spacer grid [19], [21].

4.2. Velocity and Turbulence Measurements

Turbulent velocity measurements were performed at axial locations $L/D_h=3$, 9, 16, 38 and 47 (Figure 4) and transverse Path A, B, C and Gap G (Figure 8) using one-component He-Ne LDV system.

Spacer grids disturb the local velocity fields, which causes the change of mass flow of each subchannel through spacer grids. In order to obtain a better understanding about spacer grid effects on flow mixing, mass flow separation and its redistribution behind spacer grids were investigated.

Figures 9 and 10 show the axially developing velocity profiles. The velocity in wall subchannels is larger than those in inner subchannels, which is due to the larger flow area in wall subchannels. Near the upstream spacer grid, at $L/D_h=3$, flow fluctuates significantly due to the flow blockage and turbulence generation induced by the sharp edge of the spacer grid. We can deduce the axially developing and developed region in Figures 9 and 10. The region, $L/D_h\approx38$, is the starting point of the developed region. Figure 11 shows the axial velocity profiles at Path A, B and C. The velocities have the different profiles. The velocities at Path C show a smaller magnitude than those at Path A and B. Figure 12 is the constant velocity contours in fully developed region. Near the rod surface and housing wall the velocities decrease. And a secondary flow can be seen in inner region.

Axial velocities near the wall at Path A, B, and G were plotted by wall coordinates [Figures 13 and 14] and compared with logarithmic law [22]. In Figures 13 and 14, the logarithmic equations,

$$U^+=2.44ln\ y^+ +5.0 \quad (11)$$

and

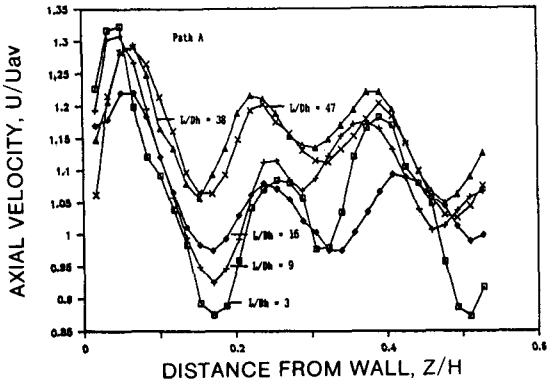

Fig. 9. Axial Velocity Profiles of the Various Elevation in Path A (Type 1)

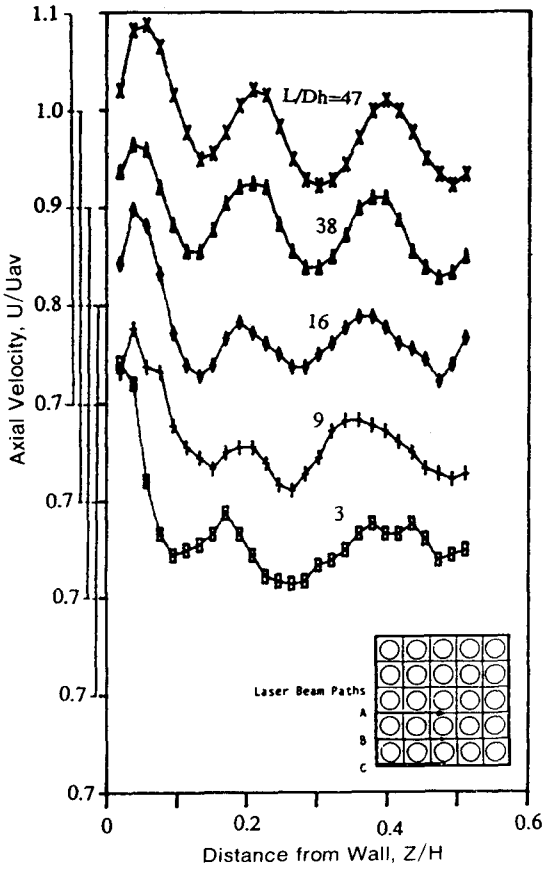

Fig. 10. Axial Developing Velocity Profiles for Standard Spacer Grid in Path A

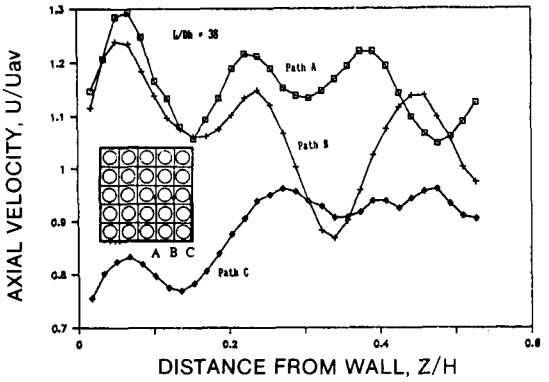

Fig. 11. Axial Velocity Profile in Path A, B and C (Type 1)

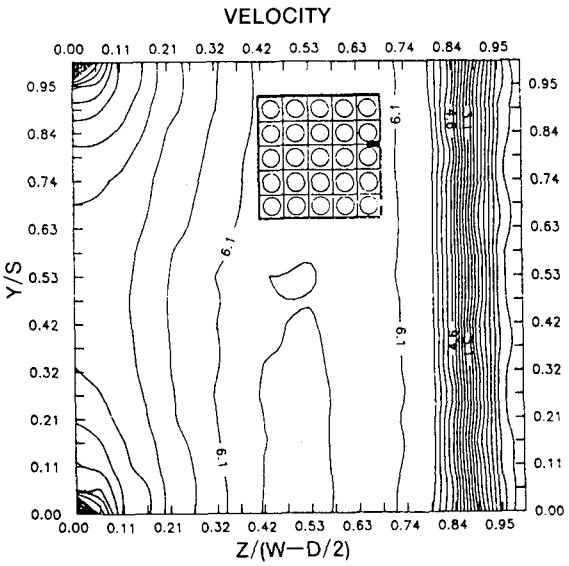

Fig. 12. Constant Velocity Contours at the Shaded Region
(Re=78300, Unit : m/sec, Type 1)

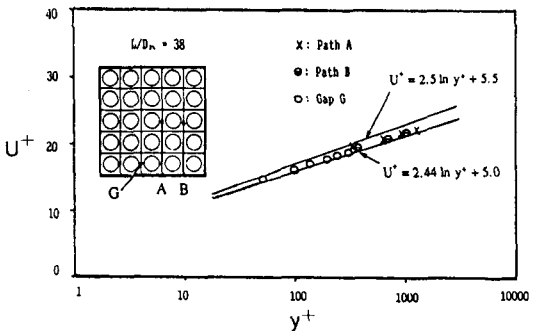

Fig. 13. Axial Velocity Profiles Near Wall in Wall Coordinate (Type 1)

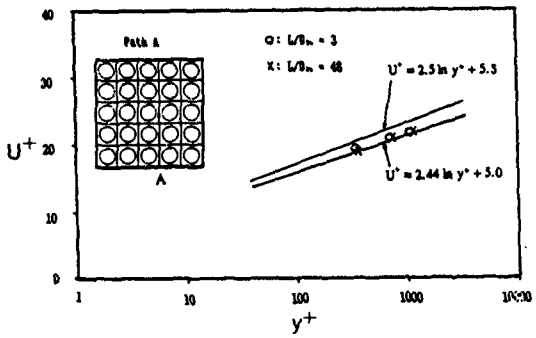

Fig. 14. Axial Velocity Profiles Near Wall in Wall Coordinate (Type 1)

$$U^+=2.5ln\ y^+ +5.5 \quad (12)$$

are for the Couette flow and the circular tube flow near wall, respectively. The data are distributed in between two equations. In Figures 13 and 14 U^+ and y^+ are defind as follows:

$$U^+=U/U^* \quad (13)$$

$$y^+=yU^*/\nu \quad (14)$$

where U^*, y, ν are a friction velocity, distance from wall, and fluid kinematic viscosity, respectively. Assuming local shear stress value in this geometry is not seriously deviated from the near wall shear stress, friction velocity can be calculated from the measured pressure drops, dP/dx, i.e.,

$$(U^*)^2=\overline{\tau_w}/\rho=-D_h/(4\rho)dP/dx \quad (15)$$

where $\overline{\tau_w}$ is time wall shear stress along the rod perimeter of primary subchannel.

Figure 15 shows the axial turbulent intensity profiles at Path A. The values in wall subchannels are larger than those in inner subchannels, which is due to the larger flow velocity field in wall subchannels.

In Figure 16, the axial turbulent intensity at gap normalized by the friction velocity was plotted and compared with Kjellstrom's [23] and Laufer's [24] data. Kjellstrom's study is from the flow in rod bundles of triangular array–the rod array of

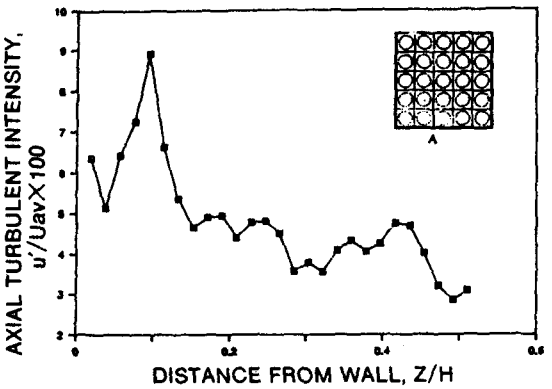

Fig. 15. Axial Turbulent Intensity at L/D_h= 47 (SSG, Type 2)

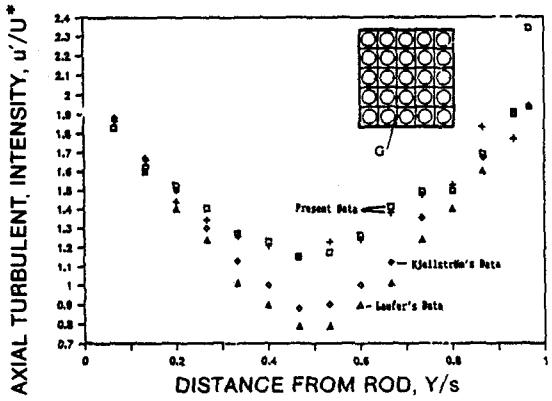

Fig. 16. Axial Turbulent Intensity Profiles Based on Friction Velocity at Gap G (L/D_h=38, □: Re=60800, + : Re=78300, Type 1)

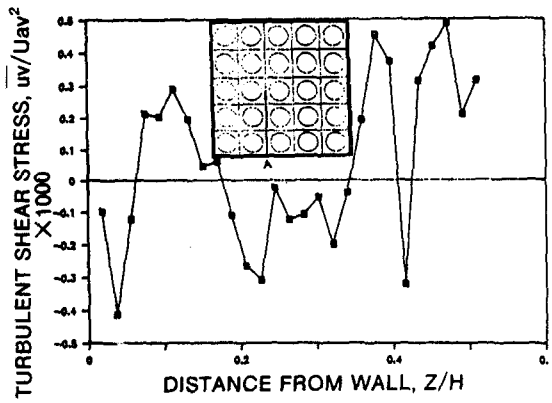

Fig. 17. Turbulent Shear Stress at L/D_h=38 (SSG, Type 2)

the present study is rectangular. And Laufer's study is in the fully developed pipe flow. Although the comparison is not for the same experimental geometry, this figure helps us obtain a better understanding of the turbulent phenomena in subchannel.

Figure 17 is the profile of the turbulent shear stresses. Turbulent shear stresses can not be measured directly by using one-component LDV system. In this study, by applying Logan's theory [25], we obtained the turbulent shear stress. The profile shows the reasonable tendency in considering the time mean velocity profiles.

4.3. Turbulent Cross-flow Mixing Rate

Turbulent cross-flow mixing rate is very significant in both the developing and the developed region. The turbulent cross-flow mixing rate effect on mixing performance between subchannels is maximized in the developed region since other effect becomes negligible relatively.

Figure 18 is for the mixing Stanton unmbers at Gap G. The Inverted Vane spacer grid shows the largest mixing Stanton number. Fig. 19 shows the mixing Stanton number at point P with variation of distance from upstream spacer grid. Mixing Stanton numbers have the largest value near the upstream spacer grid. As the flow develops, the mixing Stanton number decreases and, above the region, L/Dh>16, the values level out. This implies that, in the developing region, the hydraulic mixing between neighboring subchannels occurs actively and, in the developed region, the hydraulic mixing occurs steadily.

5. Conclusions

In this study, the detailed hydraulic characteristics is subchannels of two types of 5×5 bare rod bundles were measured using one-component He-Ne Laser Doppler Velocimeter. The experimental results led to the following conclusions.

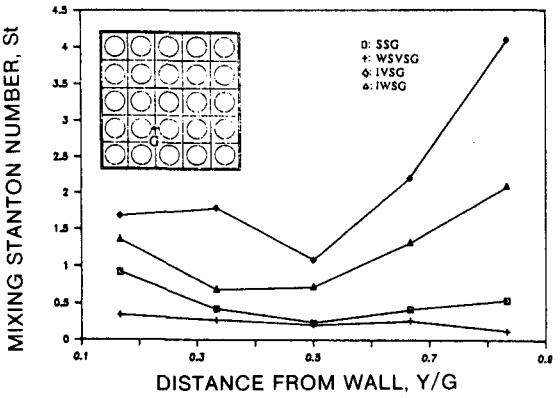

Fig. 18. Mixing Stanton Number at Gap G(L/D_h= 38, Type 2)

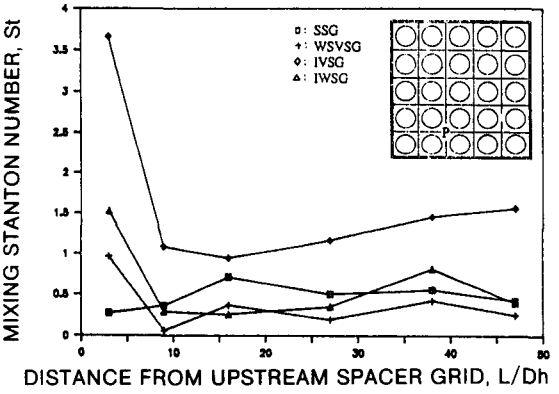

Fig. 19. Mixing Stanton Number wilh Variation of Distance From Unpstream Spacer Grid-(Type 2)

The region, $L/D_h \approx 38$, is the approximate starting point of the developed region, which implies that the upstream spacer grid influences the flow up to $L/D_h \approx 38$. Axial turbulent intensities in wall subchannels have the larger value than those in inner subchannels.

As the flow develops, the turbulent cross-flow mixing rate between neighboring subchannels decreases and, in the developed region, the values level out. This implies that, in the developing region, the hydraulic mixing occurs actively and, in the developed region, the hydraulic mixing occurs steadily.

Nomenclature

A : flow area
C_μ : turbulence constant
D : rod diameter
D_h : hydraulic diameter($4A/0_w$)
f_D : Doppler shift frequency
G : mass flux, U_{av}
G : rod gap spacing
k : turbulent kinetic energy
L : distance from upstream spacer grid
P : pitch
P : pressure
P_w : wetted perimeter
Re : Reynolds number($U_{av}D_h/\nu$)
s : rod gap spacing
St : mixing stanton number(w'/GD_h)
U : axial time mean velocity
U_{av} : channel average velocity
U^* : friction velocity
U^+ : wall coordinate velocity(U/U^*)
$\tilde{u}$: instantaneous velocity
u : axial fluctuating velocity
u′ : root mean square of u
v : radial fluctuating velocity
W : wall distance
w : azimuthal fluctuating velocity
w′ : turbulent cross-flow mixing rate per unit length
x : axial coordinate
Y : coordinate of traversing direction
y : traversing distance from wall
y^+ : wall coordinate of y(yU^*/ν)
y : centroid or mixing distance between subchannels
Z : coordinate of traversing direction
ϵ : dissipation rate of turbulent kinetic energy
κ : half angle of laser beam intersection
λ : laser wave length
ν_t : turbulent eddy viscosity
ρ : material density
$\overline{\tau}_w$: time mean wall shear stress along the rod perimeter of primary subchannel

Acknowledgements

This project was funded by the Ministry of Science and Technology. The test bundles were assembled with Zircaloy tubes obtained from KNFC and spacer grids obtained from CE and Siemens. The authors wish to express their appreciation to those companies.

References

1. M.K. Chung, S.K. Yang, and B.D. Kim, Measurements of Turbulent Flow in 5×5 PWR Rod Bundles Using Laser Doppler Velocimeter, KAERI/THD/02/89, (1989)
2. M.K. Chung, et. al., Hydraulic Tests for Mixing Grids in 5×5 Rod Bundles Using Laser Doppler Velocimeter, KAERI/TR-173/90, (1990)
3. K. Rehme, Nucl. Engrg. Des. 45, 311, (1978)
4. K. Rehme, Nucl. Engrg. Des. 62, 137, (1980)
5. K. Rehme, Nuclear Technology, 15, 148, (1982)
6. K. Rehme, Nucl. Engrg. Des. 99, 141, (1987)
7. J.D. Hooper, and K. Rehme, J. Fluid Mech. 145, 305, (1984)
8. D.S. Rowe, B.M. Johnson, and J.G. Knudson, Int. J. Heat Mass Transfer, 17, 407, (1974)
9. P. Carajilescov, and N.E. Todreas, J. of Heat Transfer, Trans. of the ASME, 101, 354, (1979)
10. M. Renksizbulut, and G.I. Hadaller, Nucl. Engrg. Des. 91, 41, (1986)
11. V. Vonka, Nucl. Engrg. Des. 106, 191, (1988)
12. V. Vonka, Nucl. Engrg. Des. 106, 209, (1988)
13. C.W. Stewart, C.L. Wheeler, R.J. Cena, C.A. McMonagle, J.M. Cuta, and D.S. Trent, COBRA-IV : The Model and the Method, BATTELLE, Pacific Northwest Laboratories, (1977)
14. B.E. Launder, and D.B. Spalding, Compt.

Methods in Applied Mech. and Engr. 3, 269, (1974)
15. H. Tennekes, and J.L. Lumley, A. First Course in Turbulence, The MIT Press, (1972)
16. J.O. Hinze, Turbulence, McGraw–Hill, 2nd. Ed. (1975)
17. F. Durst, A. Melling, and J.H. Whitelaw, Principles and Practice of Laser–Doppler Anemometry, Academic Press, (1976)
18. L.E. Drain, The Laser Doppler Technique, John Wiley and Sons, (1980)
19. K. Rehme, Nuclear Technology, Vol. 17, 15, (1973)
20. J.R. Welty, R.E. Wilson, and C.E. Wicks, Fundamentals of Momentum Heat and Mass Transfer, 2nd Ed., (1976)
21. K. Rehme, Int. J. Heat Mass Transfer, vol. 15, 2499, (1972)
22. W.M. Kays, and M.E. Crawford, Convective Heat and Mass Transfer, 2nd Ed. McGraw–Hill, (1980)
23. B. Kjellstrom, Studies of Turbulent Flow Parallel to a Rod Bundle of Triangular Array, AB Atomenergi, Studsvik, 611 01 Nykoping, Sweden, STU 68–263/u210, (1971)
24. J. Laufer, The Structure of Turbulence in Fully Developed Pipe Flow, National Advisory Committee for Aeronautics, NACA–TN–2954, (1953)
25. S.E. Logan, AIAA Journal, 10(7), 933, (1972)